Spindles, Cusps, and Bifurcation for Capsules in Stokes Flow

W. R. Dodson III[1] and P. Dimitrakopoulos[2,*]

[1]Fischell Department of Bioengineering, University of Maryland, College Park, Maryland 20742, USA
[2]Department of Chemical and Biomolecular Engineering, University of Maryland, College Park, Maryland 20742, USA

(Received 26 April 2007; revised manuscript received 11 June 2008; published 12 November 2008)

Interfacial dynamics of membrane-enclosed fluid volumes in viscous flows is complicated due to the coupling of the fluid dynamics with the membrane properties. Based on computational investigation via our interfacial spectral boundary element algorithm, our study shows that a (strain-hardening) Skalak-type capsule in a planar extensional Stokes flow develops steady-state shapes whose edges from spindled become cusped with increasing flow rate owing to a transition of the edge tensions from tensile to compressive. A bifurcation in the steady-state shapes is also found (i.e., existence of both spindled and cusped edges for a range of high flow rates) by implementing different transient processes, owing to the different evolution of the membrane tensions.

DOI: 10.1103/PhysRevLett.101.208102 PACS numbers: 87.16.dm, 82.40.Bj, 83.80.Lz, 87.16.A−

The study of the interfacial dynamics of artificial or physiological capsules (i.e., membrane-enclosed fluid volumes) in Stokes flow has seen an increased interest during the last few decades due to their numerous engineering and biomedical applications. Artificial capsules are commonly used in the pharmaceutical, food, and cosmetic industries for the controlled release of medical agents, aromas, or flavors [1]. In addition, the motion of red blood cells through vascular microvessels has long been recognized as a fundamental problem in physiology and biomechanics [2]. In this work, we restrict our interest to elastic membranes with shearing and area-dilatation resistance but negligible bending resistance. This class represents a wide range of artificial capsules. Experimental findings for biocompatible alginate capsules [3], synthetic polysiloxane [4], and aminomethacrylate capsules [5] compare very well with theoretical models that ignore bending resistance.

Current understanding of capsule dynamics at high flow rates is rather limited. Experimental findings have suggested a wealth of possible configurations, including stable steady-state shapes whose edges become rounded, then more extended but still concave (i.e., spindled), and finally cusped as the flow rate increases as shown in Fig. 6 of the work by Barthès-Biesel [6] and included here in Fig. 1(b). (It is of interest to note that the cusped shape at high flow rates reveals that the membrane has negligible bending resistance.) The transition from spindled-to-cusped edges may also be expected based on the similar transition found for low-viscosity drops or bubbles [7]. Existing analytical and computational studies are unable to predict (and thus provide physical insight on) the spindled and cusped interfacial shapes observed in experiments. The asymptotic solutions for initially spherical capsules by Barthès-Biesel and co-workers are restricted to small deformations [8]. The state of the art (low-order) three-dimensional computational methodologies are unable to find stable steady-state capsule shapes at high flow rates. These methodologies either predict interfacial breaking even at moderate flow rates [9,10] or are restricted to moderate interfacial deformations with rounded shapes [11].

To contribute to the physical understanding in this area, we utilize our interfacial spectral boundary element algorithm for capsules with elastic tensions [12] to study large deformations, in a planar extensional Stokes flow $\boldsymbol{u}^{\infty} = G(x, -y, 0)$ (where G is the shear rate), of a capsule made from a strain-hardening membrane. Our membrane description is based on the well-established continuum ap-

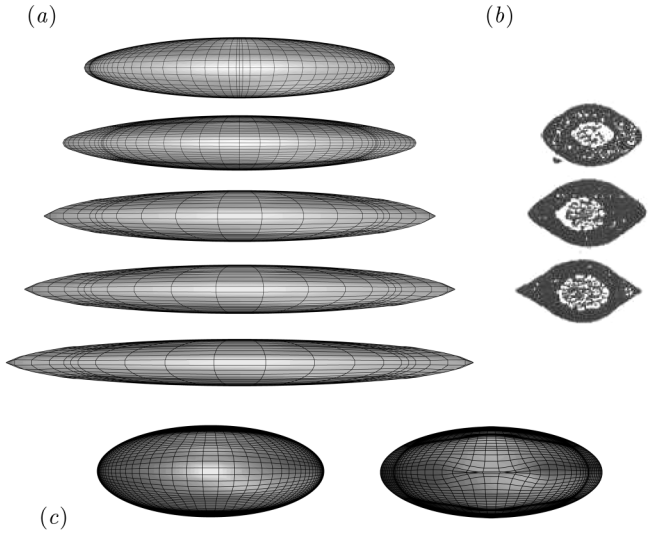

FIG. 1. (a) Steady-state shapes for a Skalak capsule with $C = 1$ and $\lambda = 1$ in a planar extensional flow, starting from a sphere, for capillary number Ca = 1, 1.5, 2, 2.5, 3. The capsules are extended along the x-direction, mainly contracted along the y-direction, while the viewpoint of the shapes shown is on the positive z-axis. (b) Steady-state profiles of a capsule (made from a polymerized polylysine membrane coated by an alginate film) in a planar extensional flow reported in Fig. 6 of the work by Barthès-Biesel [6]. (c) A close view of the spindled and cusped edges is shown for Ca = 1.5 and Ca = 2, respectively.

proach and the theory of thin shells [1,10]. Typical membrane thickness ranges from $O(\mu m)$ for alginate capsules [3], to $O(nm)$ for synthetic polysiloxane capsules [4] (i.e., it is several orders of magnitude smaller than the size of the capsule), and thus the thin-shell theory has proven to be an excellent description of these membranes [1,3–5]. To describe a strain-hardening membrane, we use the Skalak constitutive law which accounts for both shearing and area-dilatation, and while originally developed to describe biological membranes (such that of the erythrocyte), it can also be employed to model membranes obtained by interfacial polymerization [1,13].

The surface stress on the membrane is determined by the in-plane tensions, i.e., $\Delta \boldsymbol{f} = -\boldsymbol{\nabla}_s \cdot \boldsymbol{\tau}$, where the in-plane tension tensor $\boldsymbol{\tau}$ is described by the Skalak constitutive law which relates $\boldsymbol{\tau}$'s eigenvalues (or principal elastic tensions τ_α^P, $\alpha = 1, 2$) with the principal stretch ratios λ_α by

$$\tau_1^P = \frac{G_s \lambda_1}{\lambda_2}\{\lambda_1^2 - 1 + C\lambda_2^2[(\lambda_1\lambda_2)^2 - 1]\} \qquad (1)$$

(To calculate τ_2^P, reverse the λ_α subscripts.) [1,10]. The shearing modulus G_s and the area-dilatation modulus K introduce the (elastic) capillary number $\mathrm{Ca} = \mu G a/G_s$ (as the ratio of viscous forces in the fluid to shearing forces in the membrane) and the dimensionless area-dilatation modulus $C \sim K/G_s$. Here, μ is the viscosity of the surrounding fluid, and a is the length scale, i.e., the radius of a sphere with the same volume as the capsule, $V = 4\pi a^3/3$. In this Letter, we investigate capsules with $C = 1$ and equiviscosity interior and surrounding fluids (i.e., viscosity ratio $\lambda = 1$). The time is scaled with the flow time scale G^{-1} while the reported membrane tensions are scaled with G_s; the capsule's equilibrium shape under quiescent conditions (i.e., the elastic reference shape) is spherical.

The numerical solution of the interfacial problem is achieved through our interfacial spectral boundary element method for membranes [12]. The initial spherical interface is divided into a moderate number N_E of elements (e.g., see Figs. 1(a) and 3]; on each element, all geometric and physical variables are discretized using $(N_B - 1)$-order Lagrangian interpolation based on the zeros of orthogonal polynomials. This yields the spectral convergence associated with the orthogonal polynomial expansion. The accuracy of our results was verified by employing smaller time steps and different grid densities for several representative cases. (In particular, we employed $N_E = 6, 10, 14$ spectral elements with $N_B = 10$–14 basis points; for the time integration, we employed the 4th-order Runge-Kutta scheme with time step in the range $\Delta t = 10^{-4} - 10^{-3}$.) More details on our interfacial spectral boundary methods may be found in our earlier publications [14].

Figure 1(a) shows the steady-state shapes we obtain for several capillary numbers Ca by starting from quiescent initial conditions (i.e., a spherical configuration) and applying a steady flow rate Ca. Observe that for $\mathrm{Ca} = 1$, the shape shows rounded edges while for $\mathrm{Ca} = 1.5$, the edges are more pointed (i.e., the shape is spindled); at higher flow rates, the shapes become cusped. Thus, the sequence of steady-state profiles is (qualitatively) similar to that found in experiments, shown here in Fig. 1(b). We emphasize that we are unable to make quantitative comparisons since the exact parameters in the experimental study are not known, including which constitutive law is best suited to describe the specific membrane, and the exact value of the viscosity ratio λ and the flow rates Ca for the shapes shown in the experimental photographs. (As shown in Fig. 20 of Ref. [10], polylysine membrane shows higher surface-area resistance than the Skalak membrane with $C = 1$ used in our computations; this may justify why the experimental shapes show less elongation compared to our shapes.)

Examination of the membrane tensions reveals that the appearance of cusped edges at steady state is caused by the existence of negative, or compressive, tensions near the capsule edges as shown in Fig. 2. Starting from a sphere, for any flow rate Ca, the negative minimum principal tension τ_{min}^P at early times is located at the capsule edges; this tension produces no wrinkling owing to its transient nature. For $\mathrm{Ca} = 0.5$, 1, 1.5 as the capsule reaches steady state, the tensions become positive, or tensile, everywhere on the capsule including its edges, and thus these steady-state shapes are spindled. For these shapes, τ_{min}^P is located at the capsule intersection with the z-axis. For higher flow rates ($\mathrm{Ca} = 2, 2.5, 3$), τ_{min}^P is always located at the capsule edges and reaches a steady-state negative value. The negative tensions near the capsule edges cause local compression (similar to that if we pinch the capsule edges with our fingers) which results in the formation of a dimple near the capsule edges as seen in Fig. 1(c) for $\mathrm{Ca} = 2$.

We emphasize that the value of the capillary number Ca where this transition occurs depends on how the transient dynamics reach steady-state, and thus on the specific tran-

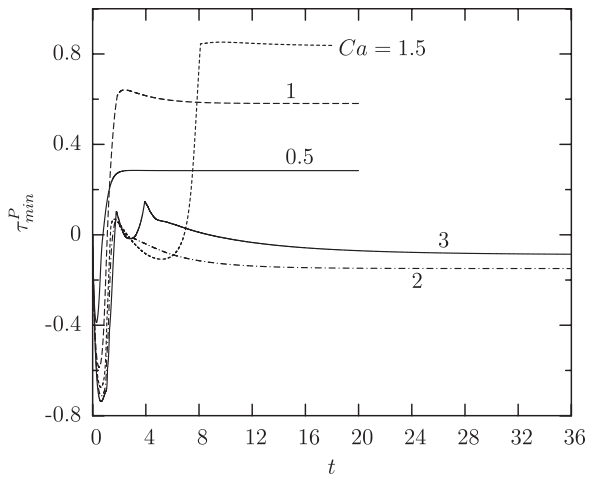

FIG. 2. Evolution of the minimum principal tension τ_{min}^P among the spectral discretization points for a Skalak capsule in a planar extensional flow, starting from a sphere, for Ca = 0.5, 1, 1.5, 2, 3.

sient experiment, we apply to the capsule. Therefore, there could be a range of high flow rates where both spindled and cusped steady-state shapes exist. Note that our results so far represent the case where, to find the steady-state capsule shape for a given flow rate Ca, we start from a spherical geometry and apply a steady flow rate with capillary number Ca. In this type of experiment, the lowest flow rate where cusped shapes were formed is Ca = 1.75.

To find the bifurcation in the steady-state shapes (i.e., the existence of both spindled and cusped edges for a range of high flow rates), we also implemented another type of experiment. In particular, starting from the rounded shape for Ca = 1, we gradually increased the capillary number (with step size ΔCa = 0.25, 0.5) allowing the system to reach steady state after each flow rate increase. In this experiment, the steady-state shapes are spindled until Ca = 2.5 as shown in Fig. 3; for higher Ca, we obtained the cusped profiles we found earlier shown in Fig. 1. We also implemented a gradual decrease in the capillary number (with step size ΔCa = 0.25) starting from the cusped steady-state shape for Ca = 3 shown in Fig. 1. In this experiment, the steady-state shapes are cusped until Ca = 2 and spindled for lower flow rates.

To show clearly the transition from spindled-to-cusped shapes as well as the shape bifurcation, in Fig. 4, we collect our data for the minimum principal tension $\tau^P_{\min}$ and the edge curvature of the steady-state shapes for the flow rates studied. Near the end of the spindle curve, there is a large increase of the edge curvature with positive value, and thus the pointed shapes have concave (or spindled) edges as shown in Fig. 3. On the other hand, along the cusp curve, the negative tensions near the capsule edges cause local compression and dimple appearance, and thus cusped steady-state profiles with large negative edge curvature (Fig. 1). It is of interest to note that, although the shape bifurcation creates a district change in the capsule profile, it causes minimal changes in the capsule's overall dimensions.

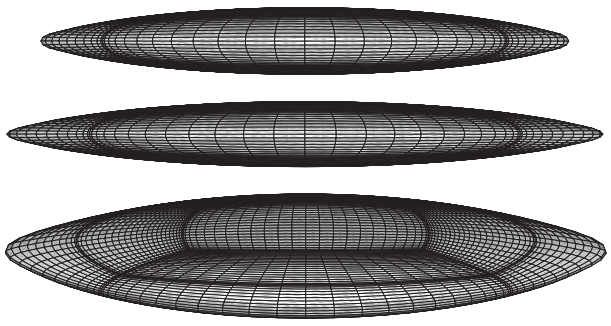

FIG. 3. Spindled steady-state shapes of a Skalak capsule for capillary number Ca = 2, 2.5. A three-dimensional view of the Ca = 2.5 shape is also included to show the flat ellipsoidal conformation of the capsule. These shapes lie in the bifurcation range 1.75 $\leq$ Ca $\leq$ 2.5 and were found by gradually increasing the flow rate.

To explain the edge evolution in these two types of experiments, we need to consider the interaction of the hydrodynamics forces with the membrane tensions. When a *spherical* capsule is let to deform in a steady flow, the restoring membrane tensions are initially weak (owing to the small interfacial deformation) but increase over time as the capsule deforms. In a moderate flow rate, the deforming hydrodynamic forces are also weak, and thus the capsule edges become monotonically more pointed over time as shown in Fig. 5 for Ca = 0.5. In higher flow rates (e.g., Ca = 1, 1.25), the stronger hydrodynamic forces overcome the weak membrane tensions, and thus initially the capsule tips become very pointed; however, after some time, the membrane tensions increase and cause a decrease of the edge curvature towards its steady-state positive value. For Ca $\geq$ 1.75, the hydrodynamic forces are so strong that cause the appearance of cusped edges via a sharp transition of the edge curvature from positive to negative as shown in the figure's inset for Ca = 2. In the second type of experiment, the gradual increase of the flow rate is accompanied by a gradual increase of the membrane

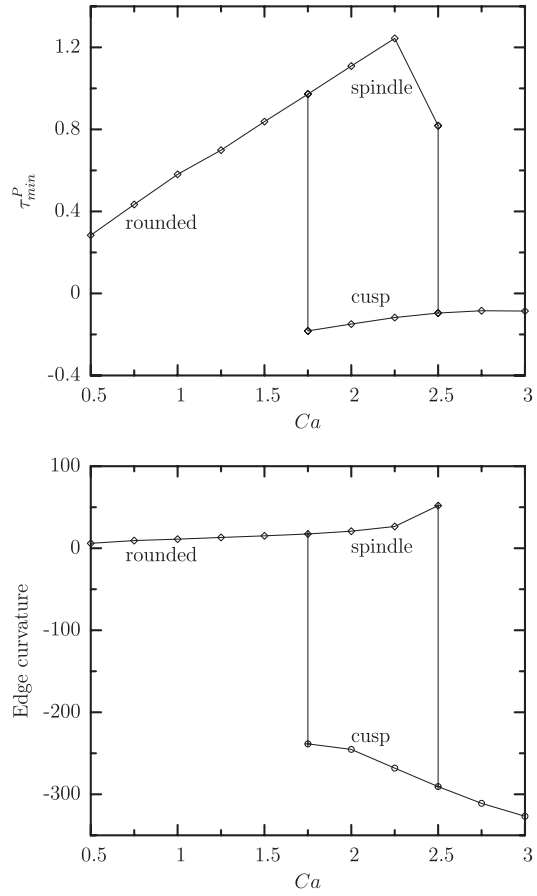

FIG. 4. Bifurcation in the dependence of (a) the minimum principal tension $\tau^P_{\min}$, and (b) the edge curvature (determined along the interfacial cross-section with the $z = 0$ plane), with the capillary number Ca, for the steady-state shape of a Skalak capsule.

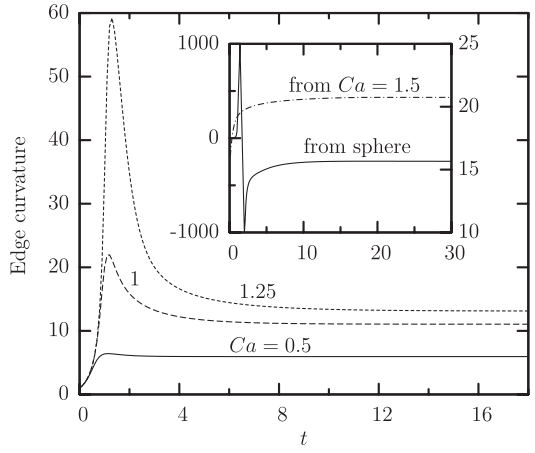

FIG. 5. Time evolution of the capsule's edge curvature for $Ca = 0.5$, 1, 1.25 starting from a sphere. The inset shows the same evolution for Ca = 2 starting from a sphere (left y-axis) and from the steady-state shape for Ca = 1.5 (right y-axis).

tensions, and thus the capsule edges become monotonically more pointed over time; this postpones the appearance of the cusped edges until $\mathrm{Ca} > 2.5$. Therefore, the different evolution of the membrane tensions in the two types of experiments creates the bifurcation range for $1.75 \leq \mathrm{Ca} \leq 2.5$.

We emphasize that our results were derived for zero bending resistance; as the bending resistance increases from zero but still remains sufficiently small [e.g., the membrane shown in Fig. 1(b)], we expect that the edge transition occurs at a slightly higher flow rate.

Concluding, our computational investigation has revealed a number of new physical results and insight for the dynamics of (strain-hardening) Skalak-type capsules at high flow rates which are commonly encountered in industrial and physiological processes. [For mm-size capsules made from aminomethacrylate membranes with shearing modulus $G_s = O(10^{-2})N/m$, flow rates $\mathrm{Ca} = O(1)$ require shear stress $\mu G = O(10)$ Pa [5].]

First, we found that as the flow rate increases, the steady-state capsule edges from rounded become spindled and finally cusped. At high flow rates, the transition to cusped shapes allows the capsule to withstand the increased hydrodynamic forces, as found for low-viscosity drops or bubbles in strong extensional Stokes flows. Thus, our present work complements the similar evolution for low-viscosity drops which was first identified by the famous experiments of G. I. Taylor in 1934, further explained in the 1970's and 1980's and still finds useful applications nowadays [7]. Second, the spindled-to-cusped shape transition is possible via the appearance of compressive tensions near the capsule edges at high flow rates; unlike earlier studies [10], our work shows that these compressive tensions do not cause interfacial breaking. Third, a bifurcation in the steady-state shapes is also found (i.e., existence of both spindled and cusped edges for a range of high flow rates) by implementing different transient processes, e.g., gradual and large change of the flow rates, owing to the different evolution of the membrane tensions. We emphasize that such bifurcation does not exist for low-viscosity drops since large flow rate increases cause instability and interfacial breaking.

Our work elucidates the importance of compressive tensions in capsule mechanical deformation as also found recently in biophysical processes, e.g., in the case of a fluid vesicle undergoing lipid uptake [15]. We hope that our study provides motivation for more experiments with capsules at high flow rates; in such a case, the experimental studies should monitor the capsule from different viewangles to capture the details of the three-dimensional interfacial shape as seen in Fig. 1.

This work was supported in part by the National Science Foundation. Helpful discussion with Professor Adomaitis and Professor Zafiriou at the University of Maryland is acknowledged. Most computations were performed on multiprocessor computers provided by the National Center for Supercomputing Applications Applications (NCSA) in Illinois.

*dimitrak@umd.edu

[1] *Modeling and Simulation of Capsules and Biological Cells*, edited by C. Pozrikidis (Chapman and Hall, London, 2003).
[2] O. K. Baskurt and H. J. Meiselman, Seminars in Thrombosis and Hemostasis **29**, 435 (2003); A. S. Popel and P. C. Johnson, Annu. Rev. Fluid Mech. **37**, 43 (2005).
[3] M. Carin, D. Barthès-Biesel, F. Edwards-Lévy, C. Postel, and D. C. Andrei, Biotechnol. Bioeng. **82**, 207 (2003).
[4] M. Husmann, H. Rehage, E. Dhenin, and D. Barthès-Biesel, J. Colloid Interface Sci. **282**, 109 (2005).
[5] G. Pieper, H. Rehage, and D. Barthès-Biesel, J. Colloid Interface Sci. **202**, 293 (1998).
[6] D. Barthès-Biesel, Physica A (Amsterdam) **172**, 103 (1991).
[7] G. I. Taylor Proc. R. Soc. A **146**, 501 (1934); J. D. Buckmaster, J. Fluid Mech. **55**, 385 (1972); A. Acrivos and T. S. Lo, *ibid.* **86**, 641 (1978); J. W. Ha and L. G. Leal, Phys. Fluids **13**, 1568 (2001).
[8] D. Barthès-Biesel, J. Fluid Mech. **100**, 831 (1980); D. Barthès-Biesel and J. M. Rallison, *ibid.* **113**, 251 (1981); D. Barthès-Biesel and H. Sgaier, *ibid.* **160**, 119 (1985).
[9] C. Pozrikidis, J. Fluid Mech. **297**, 123 (1995).
[10] E. Lac, D. Barthès-Biesel, N. A. Pelekasis, and J. Tsamopoulos, J. Fluid Mech. **516**, 303 (2004).
[11] S. Ramanujan and C. Pozrikidis, J. Fluid Mech. **361**, 117 (1998).
[12] W. R. Dodson III and P. Dimitrakopoulos, J. Fluid Mech. (2008) (to be published).
[13] R. Skalak, A. Tozeren, R. P. Zarda, and S. Chien, Biophys. J. **13**, 245 (1973).
[14] Y. Wang and P. Dimitrakopoulos, Phys. Fluids **18**, 082106 (2006); P. Dimitrakopoulos, J. Comput. Phys. **225**, 408 (2007).
[15] J. Solon, J. Pécréaux, P. Girard, M.-C. Fauré, J. Prost, and P. Bassereau, Phys. Rev. Lett. **97**, 098103 (2006).